We are IntechOpen,
the world's leading publisher of Open Access books
Built by scientists, for scientists

6,900
Open access books available

185,000
International authors and editors

200M
Downloads

Our authors are among the

154
Countries delivered to

TOP 1%
most cited scientists

12.2%
Contributors from top 500 universities

CLARIVATE ANALYTICS
BOOK CITATION INDEX
INDEXED

WEB OF SCIENCE™

Selection of our books indexed in the Book Citation Index
in Web of Science™ Core Collection (BKCI)

Interested in publishing with us?
Contact book.department@intechopen.com

Numbers displayed above are based on latest data collected.
For more information visit www.intechopen.com

Mechanical Design of Rotors with Surface Mounted Permanent Magnets

Simon Barrans and Levi Mallin

Additional information is available at the end of the chapter

Abstract

Electric machines with permanent magnet rotors are becoming increasingly popular due to the high power density that they offer relative to other configurations. Where the speed of rotation is high, the magnets are typically mounted on the surface of the rotor and retained by an outer sleeve. In the literature, a variety of analytical models have been proposed to aid the mechanical design process. Many of these models contain inherent assumptions about the stress and strain field in the rotor which may not always be apparent. In this article the range of rotor stress models are presented and explained and the limitations due to the inherent assumptions are investigated. This will allow the designer of such rotors to assess mechanical performance without introducing unforeseen errors.

Keywords: plane stress, plane strain, generalized plane strain, surface mounted permanent magnets, rotor stress, rotor failure, rotor sleeve

1. Introduction

High speed electric machines are increasingly being used in place of mechanical drive systems. As [1–3] observe, they are more efficient and reliable than their mechanical equivalents and have high power densities. Gerada et al. [4] observe that this makes them an attractive choice across a number of areas including flywheel energy storage and high speed spindles. A particularly demanding application is in electrically assisted turbochargers [5].

In order to achieve the increasingly high speeds being demanded by a number of applications, synchronous machines with permanent magnet rotors are typically used. These machines can be broadly categorized as having interior permanent magnets (IPM's) embedded within the

iron core of the rotor or surface-mounted permanent magnets (SPM) attached to the outer surface of the rotor. When considering the mechanical design of these rotors, SPM rotors allow higher rotational speeds than IPM rotors and will be the focus of this article.

The materials used for the permanent magnets include samarium cobalt (SmCo5 or Sm2-Co17) and neodymium (Nd2Fe14B). These materials are formed from sintering or bonding and are typically very weak in tension. If the magnets were simply glued to the outer surface of the rotor, the tensile stresses induced by rotation would cause them to fail. They are therefore typically retained onto the rotor shaft or core with a sleeve, as shown in **Figure 1**. The interference fit between the sleeve and the magnets places the magnets into compression. A sufficiently large interference will ensure that this initial compressive state will prevent tensile stresses being generated under rotation. However, a large interference can induce large circumferential forces in the sleeve. Increasing the sleeve thickness increases the effective air gap between the rotor and the stator which reduces electromagnetic efficiency. The mechanical design of SPM rotors is therefore challenging and has been approached in a number of ways using both analytical and numerical approaches: The analytical approaches treat the sleeve as either a thin walled or thick walled cylinder. Where a thick walled cylinder approach is used, it may be approximated as being in plane stress, plane strain or generalized plane strain. All of these approaches incorporate some degree of approximation which may limit their applicability to a particular rotor design. This article will explore these approximations and limitations.
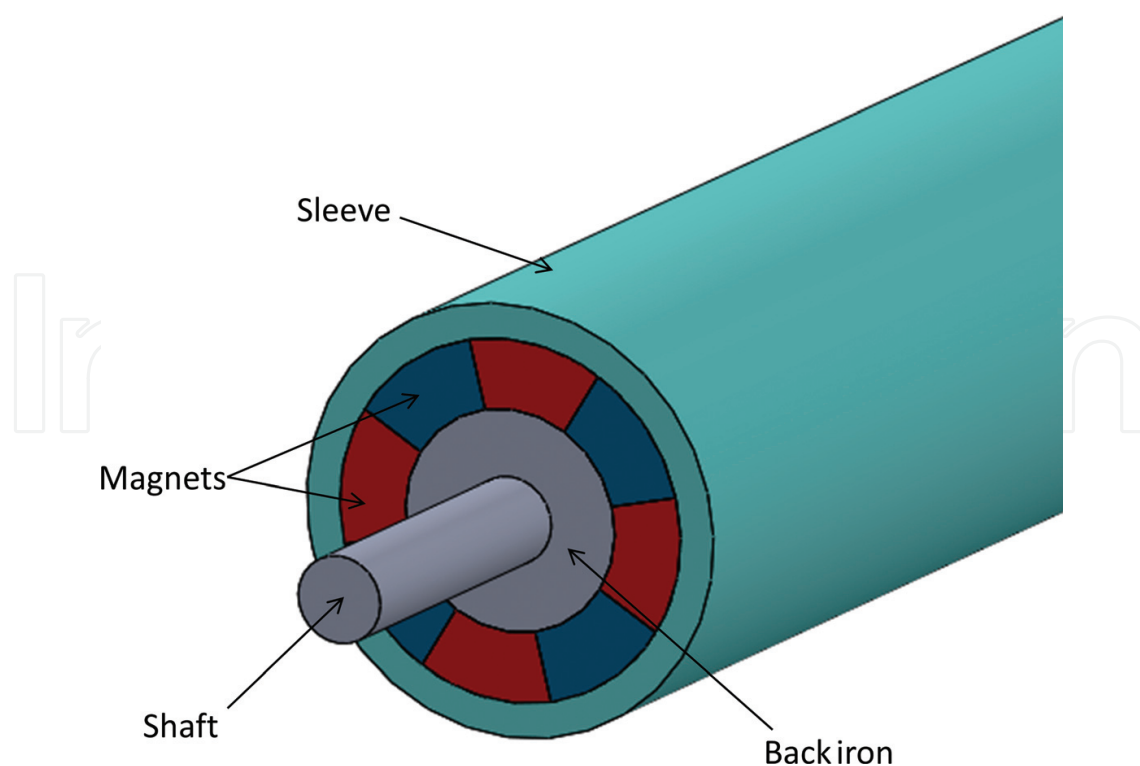
Figure 1. SPM rotor assembly.

2. Classical analytical methods

2.1. Thin shell approach

One of the simplest approaches to SPM rotor mechanical design is to assume that the sleeve acts as a thin walled cylinder, wall thickness t and radius R, as proposed in [6] and illustrated in **Figure 2**. When the rotor is stationary, the radial interference, δ, between the sleeve and the magnets generates a circumferential strain, ε_θ and stress, σ_θ, in the rotor and an interference pressure, S, between the sleeve and the magnets, given respectively by Eqs. (1)–(3).

$$\varepsilon_\theta = \frac{\delta}{R} \tag{1}$$

$$\sigma_\theta = E\varepsilon_\theta = E\frac{\delta}{R} \tag{2}$$

$$S = \frac{\sigma_\theta t}{R} = \frac{E\delta t}{R^2} \tag{3}$$

where E is the Young's modulus of the sleeve material. It is important to note here that all the deformation required to assemble the sleeve onto the magnets is assumed to take place in the sleeve, i.e. the magnets, back iron (if present) and shaft are assumed to be rigid.

The 'thin walled' cylinder approximation used here assumes that there is no variation in circumferential stress and strain through the thickness of the sleeve. Hence, in Eq. (1)–(3) only a single value for these factors is generated. The rather misleadingly termed 'thick walled' cylinder approach correctly allows for variation in stress and strain through the sleeve wall. The 'thin walled' model is therefore an approximation to the 'thick walled' model and for any
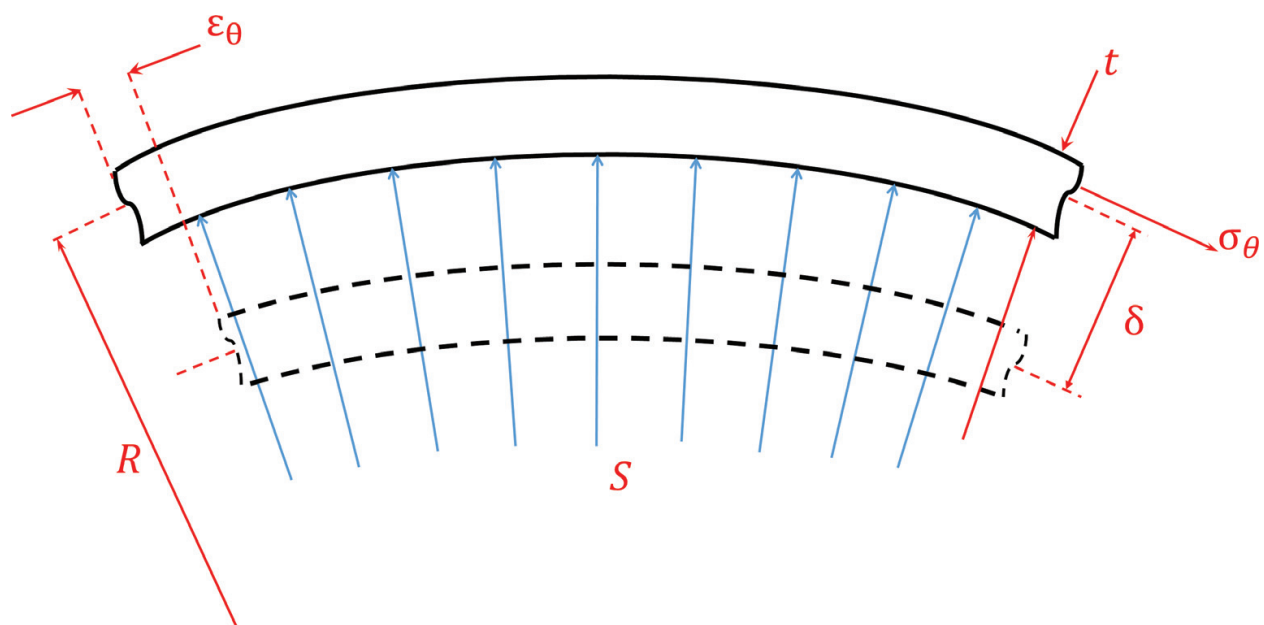
Figure 2. Thin cylinder theory.

sleeve thickness, will introduce an error in the calculation of interference pressure. The various forms of the thick walled cylinder approach will be discussed in the following sections. Taking either the plane stress approach or the generalized plane strain approach gives the relationship between interference pressure and interference as:

$$S = \frac{\delta E (R_o^2 - R_C^2)}{R_C \{ R_O^2 (1 + v) + R_C^2 (1 - v) \}} \tag{4}$$

where R_O and R_C are the outer and inner radii of the sleeve respectively and v is the Poisson's ratio of the sleeve material and the magnets, back iron and shaft are assumed to be rigid.

Assuming that the radius of the 'thin walled' sleeve, R, is the mean of the outer and inner radii:

$$R_C = R - \frac{t}{2} \text{ and } R_O = R + \frac{t}{2} \tag{5}$$

Taking typical properties for an Inconel sleeve ($E = 205$GPa, $v = 0.294$) and $\delta = 0.1$ mm, the error in the shrinkage pressure introduced by the 'thin walled' cylinder approximation is as shown in **Figure 3**. For small sleeve thicknesses, the errors are small. However, as sleeve thickness increases and sleeve diameter reduces, the thin cylinder approach significantly underestimates the circumferential stress.

Having established the interference pressure acting between the sleeve and the magnets when the rotor is stationary, the effect at maximum rotor speed must be determined. Various approaches can be taken with different criteria being used to assess the mechanical integrity of the rotor. The method proposed in [6] assumes that the interference pressure between the magnets and the back iron is the same as that between the sleeve and the magnets and then
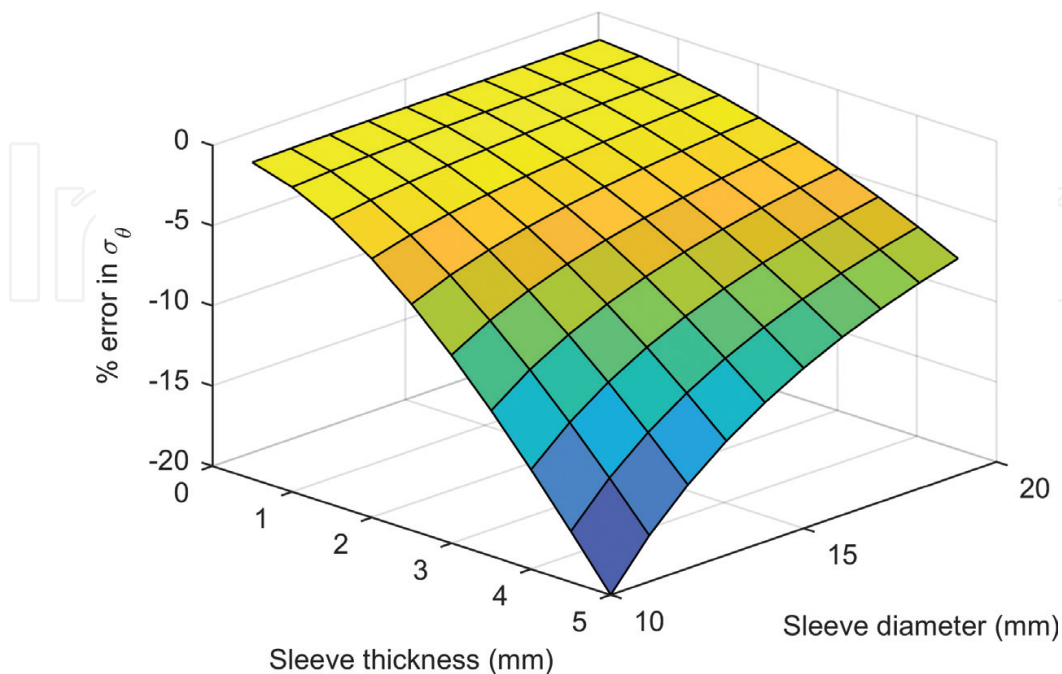
Figure 3. Thin cylinder approximation error.

determines the centripetal force required to reduce this pressure to zero (indicating that the magnets may then slip on the back iron). This approach introduces two further approximations: Firstly, to maintain force equilibrium in the radial direction, the inner surface area of the magnet must be identical to the outer surface area. Secondly, the magnets must have a sufficiently small circumferential dimension (i.e. be segmented) for no significant circumferential stress and no bending to be generated during rotation. The impact of the first effect can be readily determined and indeed can be corrected for. The impact of the second effect is more difficult to determine. If the permanent magnet is a single cylinder, it will resist circumferential expansion during rotation and there will be a smaller reduction in the interference pressure between the magnets and the back iron. However, if the magnet is formed from segments which abut in the circumferential direction, the centripetal forces will tend to separate them. This will lead to a substantial increase in the stresses in the sleeve at the point of separation and the generation of tensile stresses due to bending in the magnets. Whilst the magnet segments remain in full contact in the circumferential direction, their behavior will be identical to that of a single cylinder. This article will be restricted to rotors with magnets which are either single cylinders or are formed from segments which abut and remain in full contact during rotation.

2.2. Thick walled cylinder or disk analysis

All 'thick walled' approaches to the mechanical analysis of rotors are founded on the fundamental principles of force equilibrium, compatibility and the constitutive relationship between stress and strain within the material. These relationships are initially applied to a two dimensional
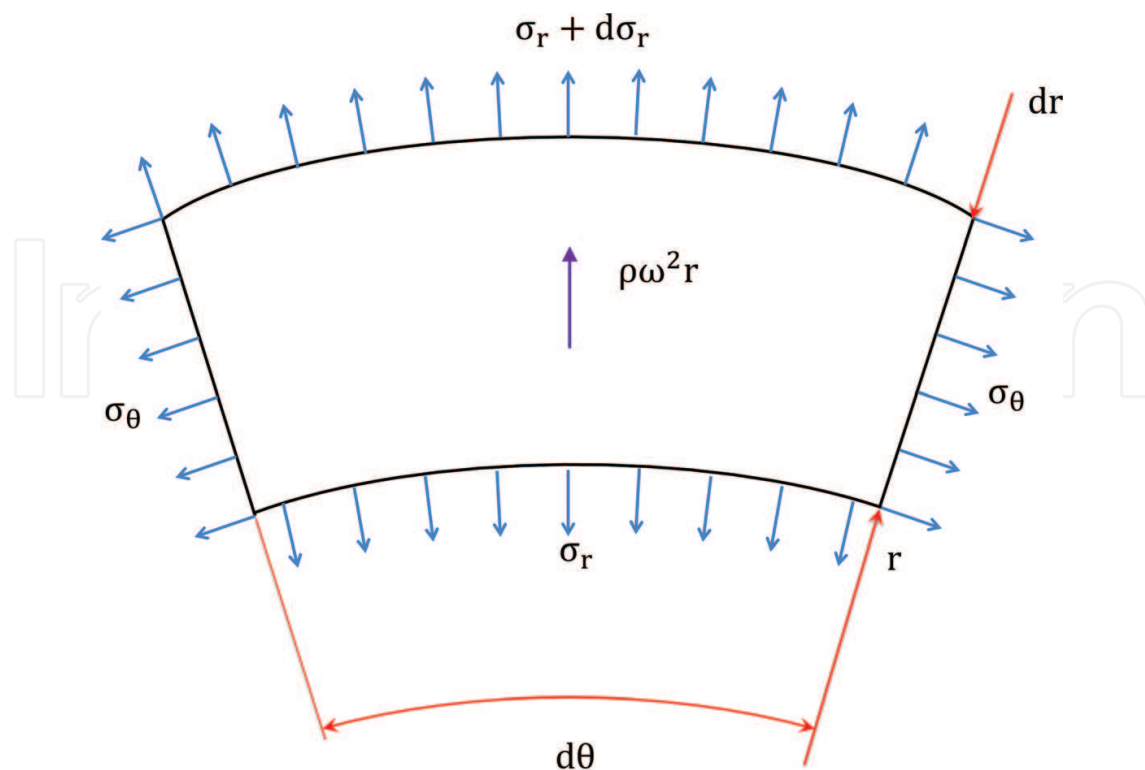

Figure 4. Internal stresses in the cylinder/disc.

cross section of the rotor, perpendicular to the axis and are presented in many text books (see for example [7]). This theoretical material is repeated here to allow the reader to appreciate the differences between the different analysis approaches.

Figure 4 shows a segment, angle $d\theta$ and thickness dr, of an annular ring, radius r, taken from a cylinder or disk which may be rotating at an angular velocity, ω, and may be subjected to either internal or external pressures. The disk material has a density, ρ. It is assumed that the radial stress, σ_r, and circumferential stress vary with radius.

Considering equilibrium of forces on this segment in the radial direction, the following relationship is obtained:

$$\sigma_\theta - \sigma_r - r\frac{d\sigma_r}{dr} = \rho\omega^2 r^2 \tag{6}$$

The constitutive relationship can then be expressed as Eqs. (7)–(9) where ε_r is the radial strain, ε_z the axial strain, α the coefficient of thermal expansion of the material and ΔT the change in temperature imposed on the material.

$$\varepsilon_r = \frac{ds}{dr} = \frac{1}{E}(\sigma_r - v\sigma_\theta - v\sigma_z) + \Delta T\alpha \tag{7}$$

$$\varepsilon_\theta = \frac{s}{r} = \frac{1}{E}(\sigma_\theta - v\sigma_r - v\sigma_z) + \Delta T\alpha \tag{8}$$

$$\varepsilon_z = \frac{1}{E}(\sigma_z - v\sigma_r - v\sigma_\theta) + \Delta T\alpha \tag{9}$$

In Eqs. (7) and (8), s is the change in radius of the segment and ds is the change in the radial dimension, as indicated in **Figure 5**.
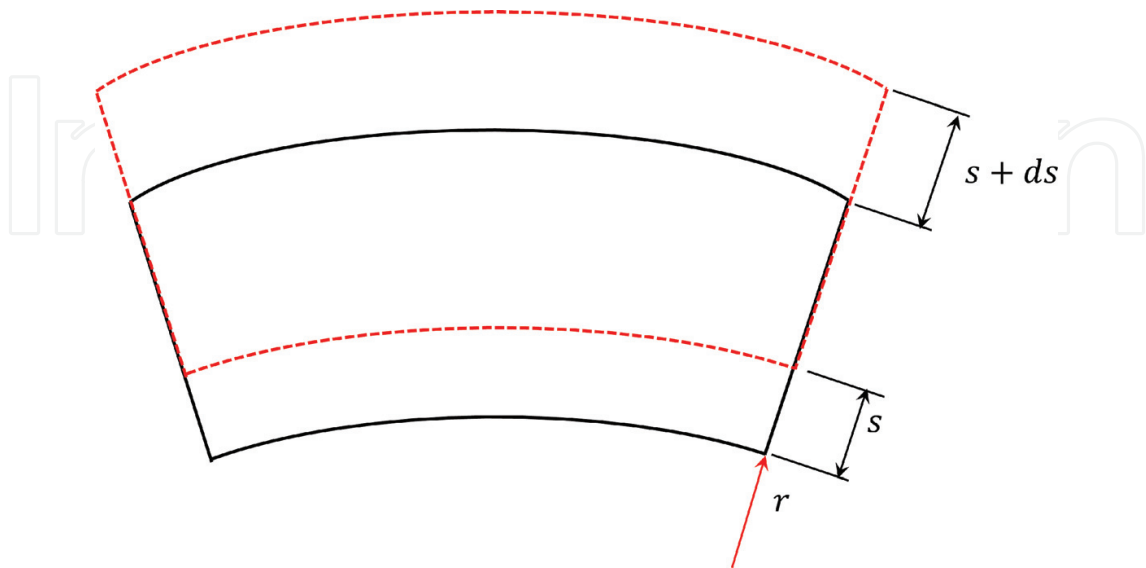
Figure 5. Change in radial dimensions of the segment.

To maintain compatibility:

$$\frac{d(r\varepsilon_\theta)}{dr} = \frac{ds}{dr} = \varepsilon_r \tag{10}$$

or, with reference to Eqs. 7 and 8:

$$(\sigma_r - \sigma_\theta)(1+v) = r\left(\frac{d\sigma_\theta}{dr} - v\left(\frac{d\sigma_r}{dr} + \frac{d\sigma_z}{dr}\right)\right) + E\alpha r\frac{d\Delta T}{dr} \tag{11}$$

As Li et al. [8] determined, the thermal barrier resisting heat transfer from the outer surface of the rotor to the air gap is much larger than the thermal resistance within the rotor components. Hence, temperatures are essentially uniform with respect to radius and vary only slightly along the axis. Assuming that $d\Delta T/dr = 0$ and combining Eq. 11 with the equilibrium equation (6), gives:

$$\frac{d\sigma_r}{dr} + \frac{d\sigma_\theta}{dr} + \frac{d\sigma_z}{dr} = -(1+v)\rho r\omega^2 \tag{12}$$

It is worth emphasizing that Eq. 12 is common to all the analytical approaches presented. However, further development of the analysis requires additional information and the solution paths diverge.

2.2.1. Plane stress approach

An approach previously used in some work [9–12] has been to assume that the axial cross section is in a state of plane stress, where $\sigma_z = 0$. Introducing this condition into Eq. (12) gives:

$$\frac{d\sigma_r}{dr} + \frac{d\sigma_\theta}{dr} = -(1+v)\rho r\omega^2 \tag{13}$$

which can be integrated to give:

$$\sigma_\theta + \sigma_r = -\frac{(1+v)\rho\omega^2 r^2}{2} + 2A \tag{14}$$

where A is a constant of integration. Reintroducing the equilibrium equation, 6, and further integrating leads to:

$$\sigma_r = A - \frac{B}{r^2} - \frac{(3+v)}{8}\rho\omega^2 r^2 \tag{15}$$

$$\sigma_\theta = A + \frac{B}{r^2} - \frac{1+3v}{8}\rho\omega^2 r^2 \tag{16}$$

with B being a further constant of integration.

In [10–12] the plane stress assumption is justified by the fact that there is no significant axial stress in the rotor as there is nothing to constrain axial extension or compression. However,

as will be demonstrated later, the lack of an external force does not prevent an axial stress being generated in the rotor under rotation. The only valid justification for the plane stress assumption is that the rotor is in the form of a disk which is of insufficient thickness for axial stress to develop.

Where the rotor is modeled as a pair of interfering cylinders, there are two sources of stress: stresses due to the interference and stresses due to rotation. Assuming linear behavior, these stresses can be determined separately and then simply summed to determine the total stress. There are also two load cases to consider:

- Stationary rotor with stress due only to interference.

- Rotating rotor with stresses generated by both rotation and interference.

For the second load case it is important to account for the change in interference due to rotation [13].

Considering **Figure 6**, the two interfering cylinders must achieve a common radius, R_c, and an interference or shrinkage pressure, S, is generated. Treating the two cylinders separately, the boundary conditions are:

$$\text{Inner cylinder}: \text{At } r = R_i; \sigma_{rii} = 0$$

$$r = R_c; \sigma_{ric} = -S$$

$$\text{Outer cylinder}: \text{At } r = R_o; \sigma_{roo} = 0$$

$$r = R_c; \sigma_{roc} = -S$$

where σ_{rii} is the radial stress in the inner cylinder at the inner radius, σ_{ric} is the radial stress in the inner cylinder at the common radius, σ_{roo} is the radial stress in the outer cylinder at the outer radius and σ_{roc} is the radial stress in the outer cylinder at the common radius.

Substituting these boundary conditions into Eq. (15) allows the constants of integration to be found and Eqs. (15) and (16) become:
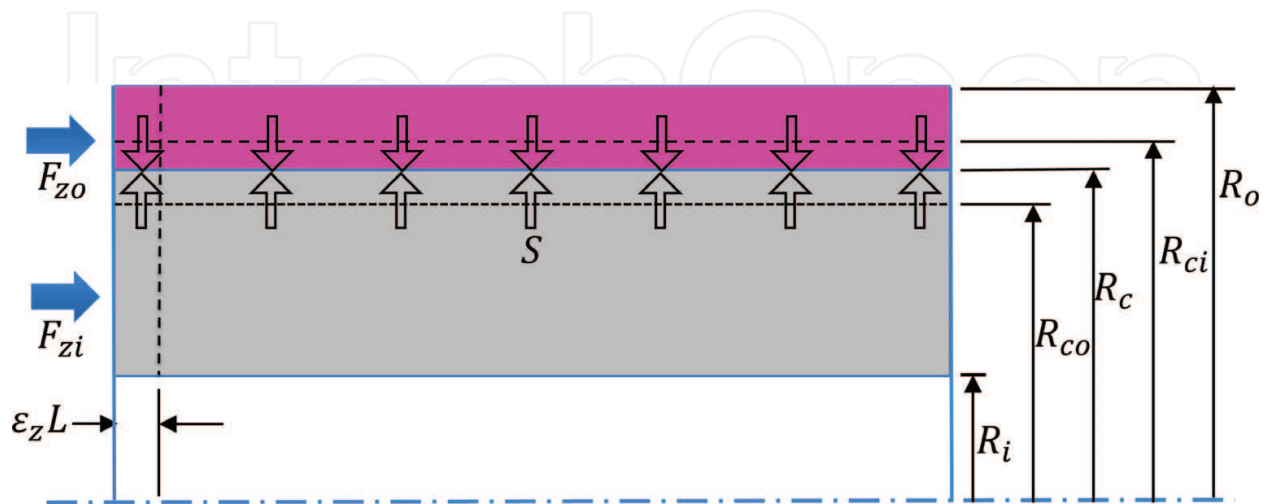
Figure 6. Interference condition.

$$\text{Inner cylinder}: \sigma_{ri} = \frac{SR_c^2}{R_i^2 - R_c^2}\left(1 - \frac{R_i^2}{r^2}\right) \tag{17}$$

$$\sigma_{\theta i} = \frac{SR_c^2}{R_i^2 - R_c^2}\left(1 + \frac{R_i^2}{r^2}\right) \tag{18}$$

$$\text{Outer cylinder}: \sigma_{ro} = \frac{SR_c^2}{R_o^2 - R_c^2}\left(1 - \frac{R_o^2}{r^2}\right) \tag{19}$$

$$\sigma_{\theta o} = \frac{SR_c^2}{R_o^2 - R_c^2}\left(1 + \frac{R_o^2}{r^2}\right) \tag{20}$$

The compatibility requirement that the two cylinders establish a common radius can be expressed as:

$$R_{ci}(1 + \varepsilon_{\theta ics}) = R_{co}(1 + \varepsilon_{\theta ocs}) \tag{21}$$

where $\varepsilon_{\theta ic}$ is the circumferential strain in the inner cylinder at the common radius, $\varepsilon_{\theta oc}$ is the circumferential strain in the outer cylinder at the common radius, R_{ci} is the outer radius of the inner cylinder prior to shrinkage and R_{co} is the inner radius of the outer cylinder prior to shrinkage.

Noting that $\sigma_z = 0$, Eqs. (17)–(20) can be used with Eq. (8) to determine the strain terms in Eq. (21) in terms of the dimensions of the cylinders and the shrinkage pressure. The shrinkage pressure can then be determined from:

$$S = \frac{R_{ci} - R_{co} + \Delta T[R_{ci}\alpha_i - R_{co}\alpha_o]}{\frac{R_{co}\{R_o^2(1+\nu_o)+R_c^2(1-\nu_o)\}}{E_o\left(R_o^2-R_c^2\right)} + \frac{R_{ci}\{R_c^2(1-\nu_i)+R_i^2(1+\nu_i)\}}{E_i\left(R_c^2-R_i^2\right)}} \tag{22}$$

where the subscripts i and o on the material properties E, ν and α indicate different properties for the inner and outer cylinders respectively.

Having determined the shrinkage pressure, the stresses due to shrinkage can be determined from Eqs. (17)–(20).

To determine the stresses due to rotation, Eqs. (15) and (16) can again be used, with the boundary conditions:

$$\text{Inner cylinder}: \text{At } r = R_i; \sigma_{rii} = 0$$

$$r = R_c; \sigma_{ric} = 0$$

$$\text{Outer cylinder}: \text{At } r = R_o; \sigma_{roo} = 0$$

$$r = R_c; \sigma_{roc} = 0$$

being used to determine the constants of integration.

2.2.2. Plane strain approach

Perhaps the first application of plane strain to the analysis of electric machine rotors is in [6] with reference to this paper being made by [14–16]. In this approach it is assumed that the axial strain is zero and therefore also that $d\varepsilon_z/dr = 0$. Hence, differentiating Eq. (9) gives:

$$\frac{1}{E}\left(\frac{d\sigma_z}{dr} - v\left(\frac{d\sigma_r}{dr} + \frac{d\sigma_\theta}{dr}\right)\right) + \alpha\frac{d\Delta T}{dr} = 0 \tag{23}$$

As before, assuming $d\Delta T/dr = 0$:

$$\frac{d\sigma_z}{dr} = v\left(\frac{d\sigma_r}{dr} + \frac{d\sigma_\theta}{dr}\right) \tag{24}$$

and introducing this into Eq. (12) gives:

$$\left(\frac{d\sigma_r}{dr} + \frac{d\sigma_\theta}{dr}\right)(1-v) = -(1+v)\rho r\omega^2 \tag{25}$$

As with the plane stress case, this equation is integrated, the equilibrium condition (Eq. (6)) reintroduced and a further integration leads to:

$$\sigma_r = A - \frac{B}{r^2} - \frac{3-2v}{8(1-v)}\rho\omega^2 r^2 \tag{26}$$

$$\sigma_\theta = A + \frac{B}{r^2} - \frac{1+2v}{8(1-v)}\rho\omega^2 r^2 \tag{27}$$

For the case of no rotation, Eqs. (26) and (27) are identical to Eqs. (15) and (16) so Eqs. (17)–(20) can be used to determine the stresses. However, with rotation present, the stresses and strains will not be the same. In order to determine the circumferential strain due to rotation (and hence the change in interference), the axial stress, σ_z, is required in Eq. (8). To determine this stress, the condition of plane strain is imposed on Eq. (9) to give:

$$\sigma_z = v(\sigma_r + \sigma_\theta) - E\Delta T\alpha \tag{28}$$

To determine the shrinkage pressure, Eqs. (26)–(28) are substituted into Eq. (8) for each cylinder at the common radius and then Eq. (21) is used to enforce compatibility between the cylinders. This leads to:

$$S = \frac{R_{ci} - R_{co} + \Delta T[\alpha_i(1+v_i)R_{ci} - \alpha_o(1+v_o)R_{co}]}{\dfrac{R_{co}\left\{R_c^2(1-v_o-2v_o^2)+R_o^2(1+v_o)\right\}}{E_o\left(R_o^2-R_c^2\right)} + \dfrac{R_{ci}\left\{R_c^2(1-v_i-2v_i^2)+R_i^2(1+v_i)\right\}}{E_i\left(R_c^2-R_i^2\right)}} \tag{29}$$

The analysis methodology is otherwise identical to that for the plane stress case with stresses due to interference and rotation being found individually and then summed. Again, as [13] observe, it is important to account for the change in interference when analyzing the combined rotation and interference load case. The impact of this can be seen in **Figure 7** for a cylinder
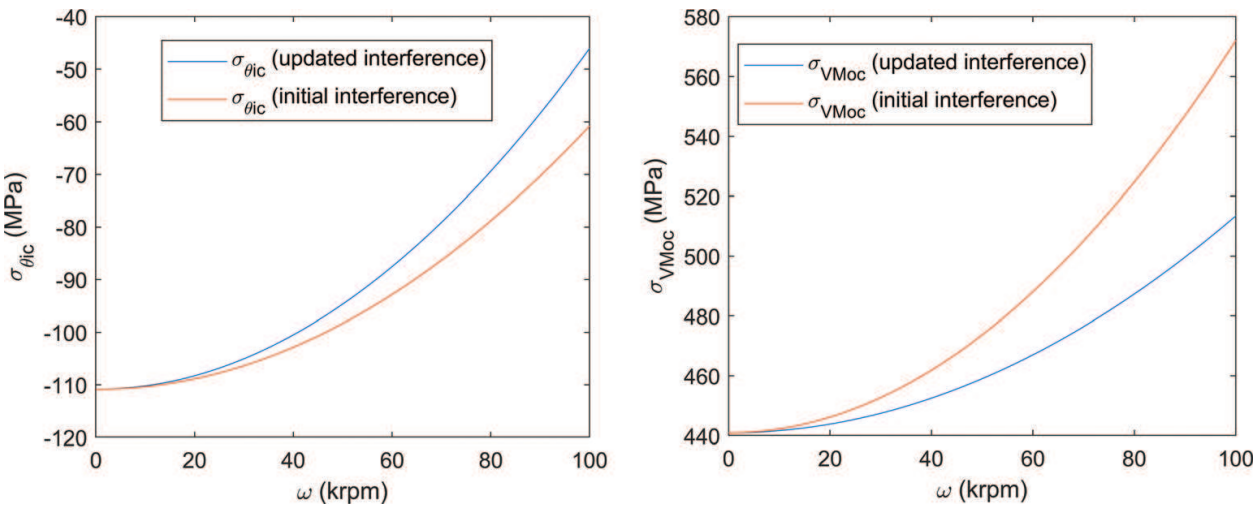
Figure 7. Impact of not updating interference.

Inner radius, R_i	6.35 mm
Common radius, R_c	11.4 mm
Outer radius, R_o	13 mm
Inner Poisson's ratio, v_i	0.27
Outer Poisson's ratio, v_o	0.284
Inner density, ρ_i	8400 kg/m^3
Outer density, ρ_o	8220 kg/m^3

Table 1. Properties for axial stress study.

pair with the properties given in **Table 1** and an initial interference of 0.03 mm. It can be seen that if the interference is not updated to account for rotation, the compressive stress at the outer radius of the magnet, $\sigma_{\theta ic}$, is overestimated and similarly, the von Mises stress on the inner radius of the sleeve, σ_{VMoc}, is overestimated as speed increases.

A criticism of the plane strain approach is the requirement for axial strain to be zero. Although a rotor assembly maybe mounted on a solid shaft with end caps to retain the magnet and sleeve, this shaft will be a deformable body. Hence, it will be possible for the rotor components to change in length.

3. Generalized plane strain approach

3.1. Axial stress generation

The generalized plane strain approach is similar to the plain strain approach and Eq. (24) can be applied. Using this in conjunction with Eq. (12), the variation of axial stress with radius is given by:

$$\frac{d\sigma_z}{dr} = \frac{-rv_i\rho_i\omega^2}{(1-v_i)} \tag{30}$$

Integrating gives the axial stress as:

$$\sigma_z = \frac{v_i\rho_i\omega^2}{2(1-v_i)}\left(C - r^2\right) \tag{31}$$

where C is a constant of integration.

Assuming that an external axial force acts on the cylinders, as indicated in **Figure 6**, and taking the inner cylinder as an example, there must be equilibrium between the internal and external axial forces, expressed as:

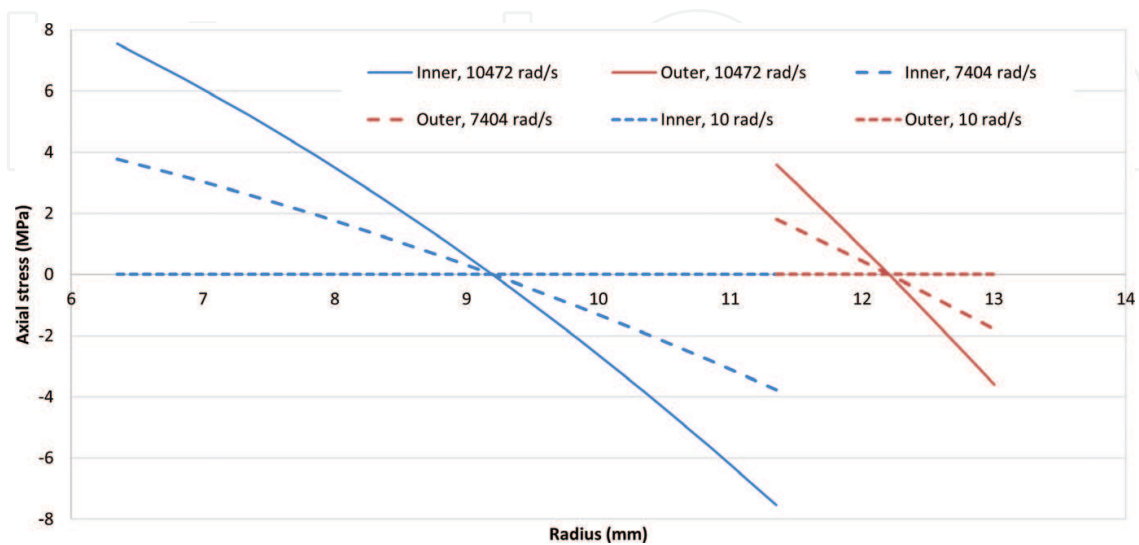$$F_{zi} = 2\pi \int_{R_i}^{R_c} r\sigma_z dr \tag{32}$$

where F_{zi} is the external axial force acting on the inner cylinder. Carrying out the integration allows the constant C to be determined and the axial stress is then given by:

$$\sigma_{zi} = \frac{F_{zi}}{\pi\left(R_c^2 - R_i^2\right)} + \frac{v_i\rho_i\omega^2}{4(1-v_i)}\left(R_c^2 + R_i^2 - 2r^2\right) \tag{33}$$

Similarly, for the outer cylinder:

$$\sigma_{zo} = \frac{F_{zo}}{\pi\left(R_o^2 - R_c^2\right)} + \frac{v_o\rho_o\omega^2}{4(1-v_o)}\left(R_c^2 + R_o^2 - 2r^2\right) \tag{34}$$

where F_{zo} is the external axial force acting on the outer cylinder.

Figure 8. Axial stress generation.

As an aside at this point, it is worth considering the possible impact of axial stress generation. Taking a cylinder pair with the dimensions and material properties shown in **Table 1** and assuming that no axial force is applied ($F_{zi} = F_{zo} = 0$), the axial stress due to rotation alone, over a range of speeds is shown in **Figure 8**. With no rotation applied, no axial stress is generated and the generalized plane strain approach is then identical to the plane stress approach. However, once rotation is introduced, axial stress is generated with peak values at the inner and outer radii. These are the positions where the circumferential strain needs to be calculated, according to Eq. (8), in order to determine the degree of interference and shrinkage pressure. The axial stress will therefore impact on these critical values.

A further point worth noting is that at the end of the cylinder axial stress cannot exist as this would place the material out of equilibrium. On the end face, a state of plane stress must exist. This change in stress state may be responsible for the end failure noted by [17].

3.2. Combining the cylinders

To account for the interaction between the cylinders, two equilibrium and two compatibility conditions need to be considered:

A. In the radial direction there must be force equilibrium at the interface between the cylinders.

B. At the interface there must be circumferential strain compatibility. With reference to **Figure 6**, this is expressed as Eq. (21).

C. Assuming that there is sufficient friction acting between the two cylinders to prevent a differential change in length, there must be axial strain compatibility. This change in length is shown in **Figure 6** as $\varepsilon_z L$ where L is the rotor length. This compatibility condition therefore becomes:

$$\varepsilon_{zi} = \varepsilon_{zo} \tag{35}$$

Where ε_{zi} and ε_{zo} are the axial strains of the inner and outer cylinders respectively.

D. There must be equilibrium of forces in the axial direction between the two cylinders. With reference to **Figure 6**:

$$F_{zi} = -F_{zo} \tag{36}$$

To enforce condition A, the constants in Eqs. (26) and (27) are determined with the shrinkage pressure, S, applied at the common radius for the inner and outer cylinders. A pair of simultaneous equations are then determined by considering conditions D and C together and then D and B together. Details of this analysis are given in [18], the result being:

$$\begin{bmatrix} U & V \\ X & Y \end{bmatrix} \begin{bmatrix} F_{zo} \\ S \end{bmatrix} = \begin{bmatrix} W \\ Z \end{bmatrix} \tag{37}$$

where:

$$U = \frac{1}{\pi}\left[E_i\left(R_i^2 - R_c^2\right) - E_o\left(R_o^2 - R_c^2\right)\right]$$

$$V = -2R_c^2\left[\nu_O E_i\left(R_i^2 - R_c^2\right) - \nu_i E_o\left(R_o^2 - R_c^2\right)\right]$$

$$W = \left(R_o^2 - R_c^2\right)\left(R_i^2 - R_c^2\right)\left\{\frac{\omega^2}{2}\left[\nu_O E_i\rho_o\left(R_c^2 + R_o^2\right) - \nu_i E_o\rho_i\left(R_c^2 + R_i^2\right)\right] + T(\alpha_i - \alpha_o)E_o E_i\right\}$$

$$X = \frac{1}{\pi}\left[\nu_i E_o R_{ci}\left(R_o^2 - R_c^2\right) + \nu_o E_i R_{co}\left(R_c^2 - R_i^2\right)\right]$$

$$Y = -\left\{E_o R_{ci}\left(R_o^2 - R_c^2\right)\left[R_c^2(1 - \nu_i) + R_i^2(1 + \nu_i)\right] + R_{co}E_i\left(R_c^2 - R_i^2\right)\left[R_o^2(1 + \nu_o) + R_c^2(1 - \nu_o)\right]\right\}$$

$$Z = \left(R_c^2 - R_i^2\right)\left(R_o^2 - R_c^2\right)\left\{E_o E_i[R_{co} - R_{ci} + T(\alpha_o R_{co} - \alpha_i R_{ci})]\right.$$

$$+ \frac{\rho_o R_{co}\omega^2 E_i}{8(1 - \nu_o)}\left[2\left(R_c^2 + 3R_o^2\right) - 4\nu_o\left(R_o^2 + R_c^2\right) - 2\nu_o^2\left(R_o^2 - R_c^2\right)\right]$$

$$\left. - \frac{\rho_i R_{ci}\omega^2 E_o}{8(1 - \nu_i)}\left[2\left(R_c^2 + 3R_i^2\right) - 4\nu_i\left(R_c^2 + R_i^2\right) - 2\nu_i^2\left(R_i^2 - R_c^2\right)\right]\right\}$$

4. Comparison of models

4.1. Basic model parameters

The material properties used in the comparison of the various models are as shown in **Table 1**, these being typical properties for samarium cobalt magnets and an Inconel sleeve. Analyses were carried out for the parameters shown in **Table 2**.

For this study temperature was not treated as a variable so thermal expansion effects were ignored.

A critical result is the circumferential stress on the outer radius of the magnet, $\sigma_{\theta ic}$, at maximum speed. This is shown in **Figure 9** for a magnet inner radius of 6 mm. When the degree of interference and sleeve thickness are low there is insufficient compression generated in the magnets by the sleeve and this stress becomes tensile. This may lead to magnet failure dependent on the precise material used. Or, if magnets are segmented, it would lead to magnet separation and localized over-loading of the sleeve.
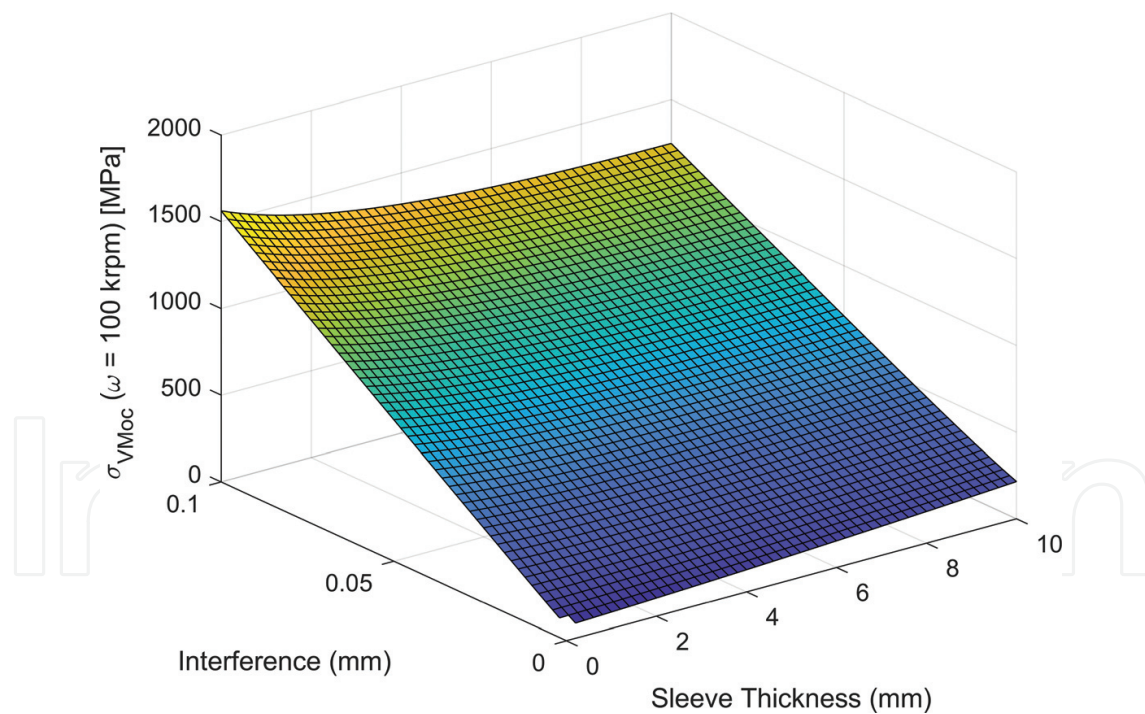
Parameter	Minimum	Maximum (or discrete values)
Magnet inner radius, R_i, (mm)		4, 6, 8
Common radius, R_c, (mm)		14
Interference, δ, (mm)	0	0.1
Sleeve thickness (mm)	0	10
Rotor speed (ω) (krpm)	0	100

Table 2. Geometric parameters for comparative study.
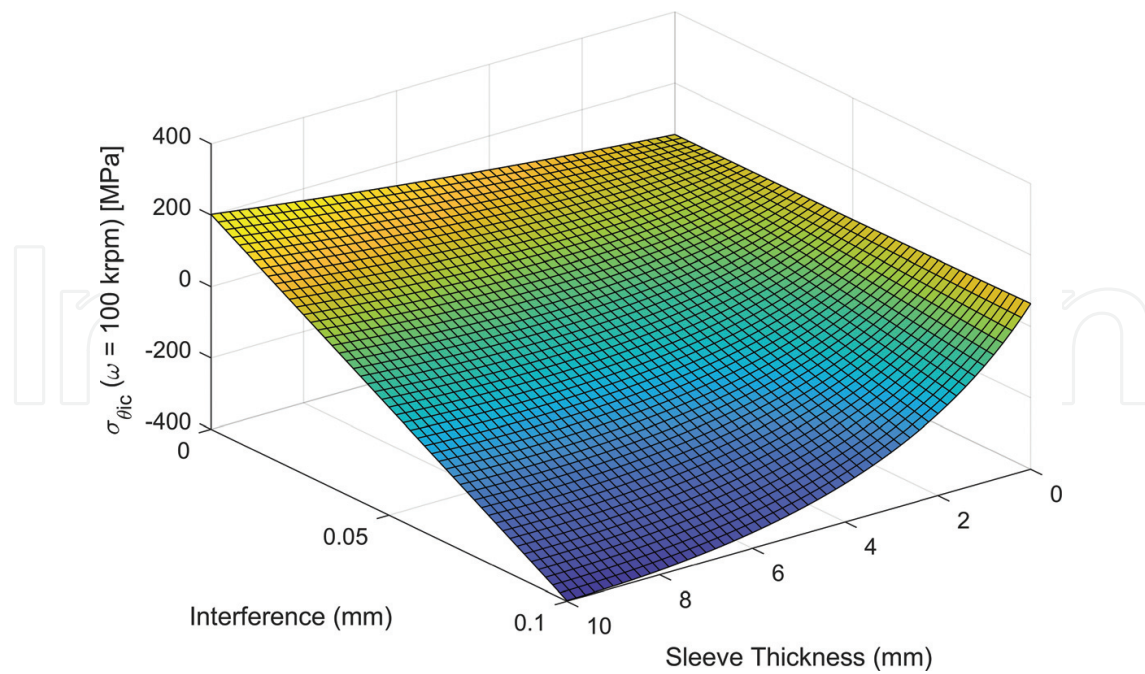
Figure 9. Circumferential stress on the magnet outer radius at speed.

Figure 10. Von Mises stress at the inner radius of the sleeve at speed.

Figure 10 shows the von Mises stress generated at the inner surface of the sleeve, σ_{VMoc}, at zero speed, again with a magnet inner radius of 6 mm. This stress or its equivalent at maximum speed will be critical for the sleeve which is normally a ductile material. This stress becomes larger as interference increases (and hence both radial and circumferential stress magnitudes increase) but reduces as sleeve thickness increases.

4.2. Comparing plane stress and plane strain models

Figure 11 shows the percentage difference in von Mises stress between the plane stress and plane strain theories at maximum speed for a rotor with a magnet inner radius of 4 mm. For smaller levels of interference, this difference is substantial. The percentage difference in circumferential
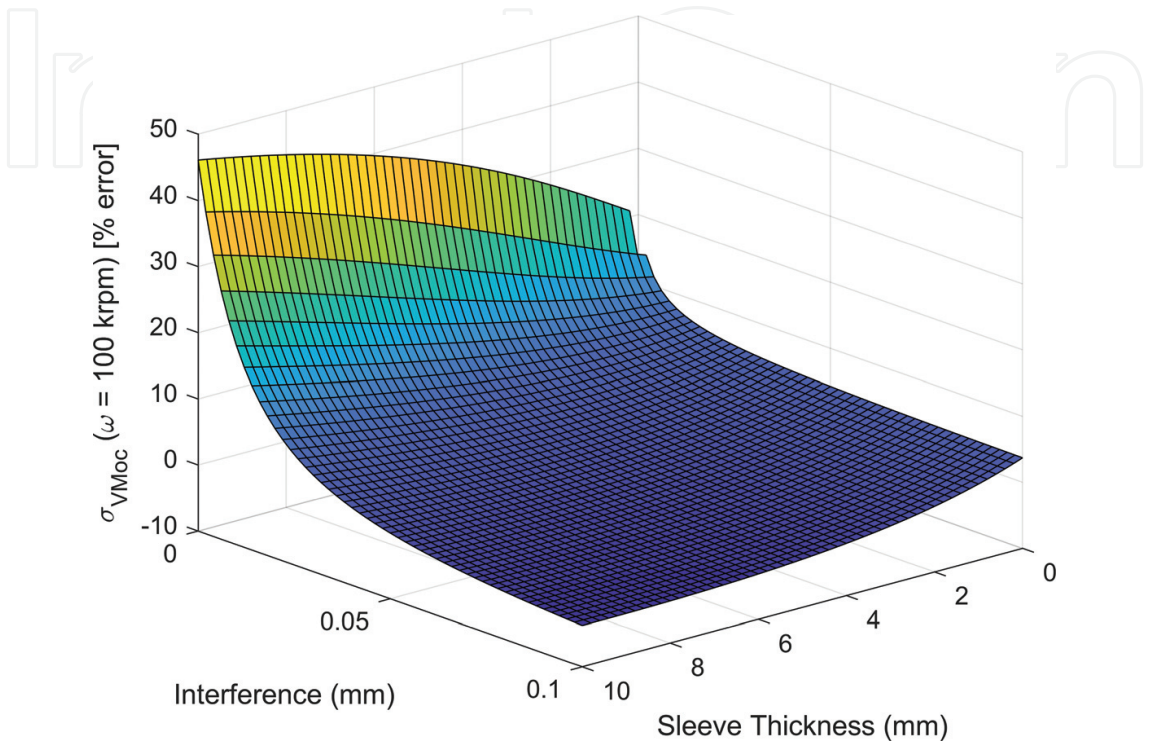

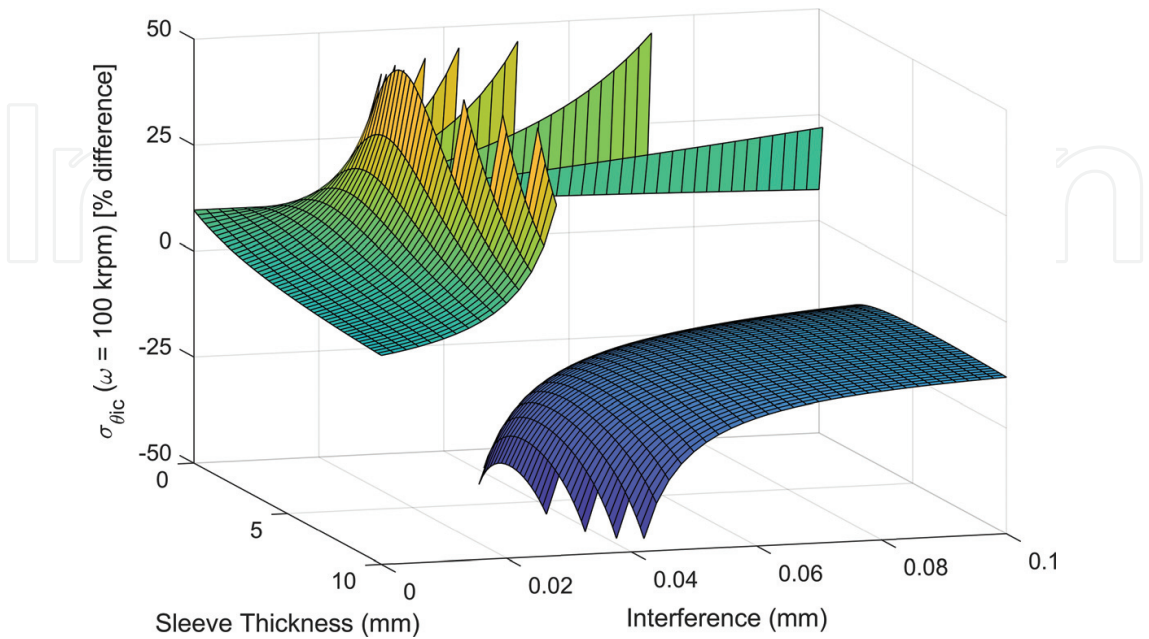**Figure 11.** Percentage difference in σ_{VMoc} at maximum speed.

Figure 12. Percentage difference in $\sigma_{\theta ic}$ at maximum speed.

stress in the magnet for the same case is shown in **Figure 12**. Where this stress approaches zero, the results approach infinity and have been omitted from the figure for clarity. In order to optimize rotor design it will be desirable to approach zero circumferential stress in the magnet as maximum speed is reached. Hence, whilst the absolute differences between the two theories are small (because the absolute values are small), they are still critical. These results highlight the need for a theoretical approach that does not incorporate the conflicting approximations of the plane stress and plane strain models.

4.3. Generalized plane strain model

The generalized plane strain model does not include any of the approximations of the plane stress or plane strain theories. For the case of relatively long cylinders with high levels of friction between the components, this theory can be regarded as accurate away from the ends of the rotor. **Figure 13**
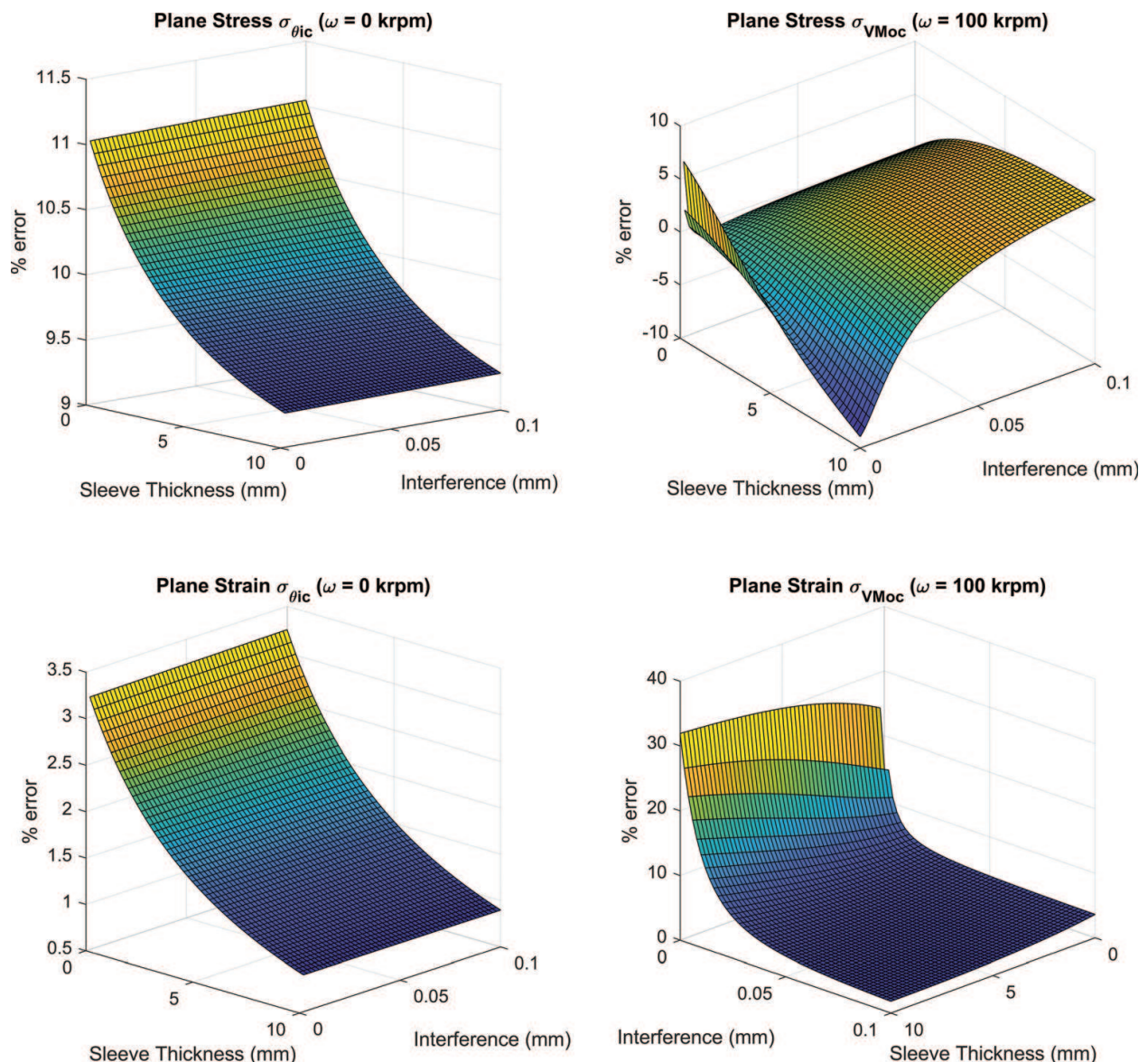
Figure 13. Errors in plane stress and plane strain theories.

shows a selection of results comparing the plane stress and plane strain models to the generalized plane strain model for a rotor with a magnet inner radius of 4 mm. When stationary the error in $\sigma_{\theta ic}$ increases with decreasing sleeve thickness for both the plane stress and plane strain models. This is much more significant for the plane stress model. Looking at the von Mises stress at maximum speed, the plane strain model shows increasing error as the interference is reduced but relatively little dependence on sleeve thickness. The error in the plane stress result is dependent on both sleeve thickness and interference but is never as large as the peak error value for the plane strain theory.

5. Conclusions and further work

The work presented here has shown that:

- Using a thin walled cylinder model for the rotor sleeve will introduce increasing errors as the sleeve thickness increases.

- Neglecting the change in interference due to rotation will introduce significant errors.

- The plane stress and plane strain models will often give similar results for rotors operating well within their design limits. However, when rotors are optimized to minimize sleeve thickness or increase speed such that the circumferential stress in the magnet becomes a limiting factor, there is significant difference between the theories. Both theories incorporate approximations which are not generally true for this application.

- The plane stress and plane strain models show significant differences from the generalized plane strain model, particularly at the design limits.

Despite avoiding the limiting approximations of the other theories, the generalized plane strain model still has limitations. Further development is required to consider:

- The impact of lower levels of friction where the cylinders may slip against each other in the axial direction.

- Situations where more than two cylinders are interfering such as with magnets affixed to a back iron and retained with a sleeve.

- Sleeves made from composite materials where the constitutive equations, 7 to 9, are not applicable in the form given here.

Author details

Simon Barrans* and Levi Mallin

*Address all correspondence to: s.m.barrans@hud.ac.uk

University of Huddersfield, UK

References

[1] Tenconi A, Vaschetto S, Vigliani A. Electrical machines for high-speed applications: Design considerations and tradeoffs. IEEE Transactions on Industrial Electronics. 2014;**61**(6): 3022-3029

[2] Fang H, Qu R, Li J, Zhang P, Fan X. Rotor design for high-speed high-power permanent-magnet synchronous machines. IEEE Transactions on Industry Applications. 2017;**53**(4): 3411-3419

[3] Li S, Sarlioglu B. Assessment of high-speed multi-megawatt electric machines. In: Presented at the Electric Machines & Drives Conference; Coeur d'Alene, ID, USA; 10–13 May, 2015

[4] Gerada D, Mebarki A, Brown NL, Gerada C, Cavagnino A, Boglietti A. High-speed electrical machines: Technologies, trends, and developments. IEEE Transactions on Industrial Electronics. 2014;**61**(6):2946-2959

[5] Lee W, Schubert E, Li Y, Li S, Bobba D, Sarlioglu B. Overview of electric turbocharger and supercharger for downsized internal combustion engines. IEEE Transactions on Transportation Electrification. 2017;**3**(1):36-47

[6] Binder A, Schneider T, Klohr M. Fixation of buried and surface-mounted magnets in high-speed permanent-magnet synchronous machines. IEEE Transactions on Industry Applications. 2006;**42**(4):1031-1037

[7] Hearn EJ. Mechanics of Materials. Vol. 2. Oxford, UK: Pergamon; 1985

[8] Li W, Qiu H, Zhang X, Cao J, Yi R. Analyses on electromagnetic and temperature fields of superhigh-speed permanent-magnet generator with different sleeve materials. IEEE Transactions on Industrial Electronics. 2014;**61**(6):3056-3063

[9] Borisavljevic A, Polinder H, Ferreira JA. Enclosure design for a high-speed permanent magnet rotor. In: Presented at the Power Electronics, Machines and Drives; Brighton, UK; 2010

[10] Zhang F, Du G, Wang T, Liu G, Cao W. Rotor retaining sleeve design for a 1.12-MW high-speed PM machine. IEEE Transactions on Industry Applications. 2015;**51**:3675-3685

[11] Zhu C, Chen L. Rotor strength analysis for stator-permanent magnet machines. In: Presented at the International Conference on Electrical Machines and Systems (ICEMS); Sydney, NSW, Australia; 2017

[12] Cheng W, Xu G, Sun Y, Geng H, Yu L. Optimum design of ultra high speed hybrid rotor of PM machines. In: Presented at the International Conference on Mechatronics and Automation; Tianjin, China; 2014

[13] Burnand G, Araujo DM, Perriard Y. Very-high-speed permanent magnet motors: Mechanical rotor stresses analytical model. In: Presented at the Electric Machines and Drives Conference (IEMDC); Miami, Florida, USA; 2017

[14] Thomas AS, Zhu ZQ, Jewll GW. Comparison of flux switching and surface mounted permanent magnet generators for high-speed applications. In: Presented at the Power Electronics, Machines and Drives (PEMD); 2011

[15] Fernando WU, Gerada C. High speed permanent magnet machine design with minimized stack-length under electromagnetic and mechanical constraints. International Journal of Applied Electromagnetics and Mechanics. 2014;**46**:95-109

[16] Tao Z, Xiaoting Y, Huiping Z, Hongyun J. Strength design on permanent magnet rotor in high speed motor using finite element method. TELKOMNIKA. Indonesian Journal of Electrical Engineering. 2014;**12**:1758-1763

[17] Smith DJB, Mecrow BC, Atkinson GJ, Jack AG, Mehna AAA. Shear stress concentrations in permanent magnet rotor sleeves. In: Presented at the International Conference on Electrical Machines; Rome, Italy; 2010

[18] Barrans S, Al-Ani M, Carter J. Mechanical design of rotors for permanent magnet high-speed electric motors for turbocharger applications. IET Electrical Systems in Transportation. 2017;**7**(4):278-286